RSC Pharmaceutics

ROYAL SOCIETY OF CHEMISTRY

PAPER

View Article Online
View Journal | View Issue

Cite this: *RSC Pharm.*, 2025, **2**, 644

Redox-responsive micellar-like nanoparticles can overcome intrinsic multi-drug resistance in tumour spheroids of triple negative breast cancer†

Cíntia J. Monteiro,‡§[a] Patrícia F. Monteiro,*‡[a] Alessandra Travanut,[a] Muhammad Gulfam,[a] David M. Heery,[a] Anna Grabowska[b] and Cameron Alexander *[a]

Triple negative breast cancer (TNBC) is one of the most difficult subtypes of breast cancer to treat, due to its aggressiveness, high heterogeneity and lack of targeted therapies. Efforts have been made to elucidate the mechanisms by which TNBC cells become drug-resistant, aiming to identify new molecular targets for the development of effective treatments. Here, we have generated a TNBC 3D multi-cellular spheroid model using MDA-MB-231 cells and assessed the efficacy of drug delivery formulations based on docetaxel (DTX)-loaded micellar-like nanoparticles (MLNP) compared with free DTX. We assessed the viability and the induction of apoptosis in the treated spheroids using established apoptosis and necrosis biomarkers: annexin-V, PI, Sytox and caspase 3 and 7 activity by flow cytometry. Given the efficacy results of the MLNPs and free DTX, the expression of selected genes related to resistance in breast cancer cells was assessed by RT-qPCR (real-time polymerase chain reaction) as well as western blot and immunofluorescence of the drug resistance protein (ABCG2/BCRP) in both 3D and 2D cell culture models of MDA-MB-231 cells. The results from these assays indicate that the TNBC 3D multi-cellular spheroids exhibit an intrinsic multi-drug resistance (MDR) through the up-regulation of ABCG2/BCRP gene and protein, compared to monolayers of the same cell line. Moreover, the results also demonstrate that the MLNPs had the best efficacy against TNBC 3D spheroids whereas the free drug was less efficacious. This suggests that the MLNPs were able to overcome the MDR of the TNBC 3D cell culture model when compared to free DTX.

Received 20th December 2024,
Accepted 28th March 2025

DOI: 10.1039/d4pm00336e

rsc.li/RSCPharma

1 Introduction

The failure of chemotherapeutic drugs can be credited to multiple factors, such as variations in absorption, metabolism and delivery of drugs to cancer cells. These mechanisms can be patient-specific when drugs are systemically administered, however the location of the tumour can contribute to the failure of the treatment when they are located in parts of the body where the drug cannot easily penetrate. In addition, tumours can be protected by the local environments as when the tumour vasculature is altered.[1] Nonetheless, the major aspect that leads to failure of cancer chemotherapy is the development of multi-drug resistance (MDR), whereby cancer cells acquire resistance to anticancer drugs.[2,3]

MDR is considered to be the major barrier against clinical success of conventional chemotherapy and it particularly affects patients with breast, ovarian, lung, blood and gastrointestinal tract cancers.[1,4,5] Tumours generally consist of distinct cancer cell populations, of which some are sensitive to specific drugs, whereas others are drug-resistant. The resistant cells survive chemotherapy, and as a consequence, the tumour grows again and subsequent chemotherapy can fail as more cells become resistant to the drugs.[4]

Established mechanisms of resistance in cancer are correlated with the increased energy-dependent efflux of certain hydrophobic drugs. This mechanism is mediated by the ATP-binding cassette (ABC) transporters, which are one of a family of energy-dependent transporters. Various members of the ABC transporters family are capable of inducing MDR, such as P-glycoprotein (Pgp, also known as *ABCB1* or MDR1),

[a]*School of Pharmacy, University of Nottingham, NG7 2RD, UK.*
E-mail: cameron.alexander@nottingham.ac.uk, patricia.monteiro@astrazeneca.com
[b]*BioDiscovery Institute, University of Nottingham, NG7 2RD, UK*

†Electronic supplementary information (ESI) available. See DOI: **https://doi.org/10.1039/d4pm00336e**

‡These authors contributed equally to the manuscript.

§Current address: Department of Pharmaceutical Sciences (FCM), University of Campinas (Sao Paulo, Brazil).

MRP1 (*ABCC1* or multidrug resistance-associated protein 1) and the human breast cancer resistance protein BCRP (*ABCG2* or ATP-binding cassette sub-family G member 2). These proteins confer resistance to a broad variety of compounds, and transport drugs which are central to chemotherapeutic treatments including breast cancer, such as, but not limited to, vinca alkaloids, anthracyclines and taxanes.[1,6,7]

Regarding the treatment of triple negative breast cancer (TNBC), neoadjuvant chemotherapy (NAC) remains the standard of care for many patients. Due to the lack of standard molecular targets in TNBC, neither hormonal therapy or nor anti-HER2 targeted agents have efficacy against these types of breast cancer.[8] Although TNBC tumours are generally susceptible to NAC there is no correlation with the overall survival of the patients. The risk of recurrence for TNBC patients in the first 3–5 years is considerably higher than for the patients with hormone positive breast cancer and overall, the prognosis of the patients is poor as compared to non-TNBC patients.[9]

Anthracyclines and taxanes are widely used in the treatment of TNBC.[10,11] However, resistance to these drugs often develops followed by metastatic disease and mortality.[12] Thus, the failure in the treatment of TNBC can be related to the resistance to the chemotherapeutic drugs. Moreover, it has been found that TNBC cells confronted by chemotherapy may adapt to become resistant.[13]

Strategies capable of overcoming multi-drug resistance in cancer treatment have increasingly adopted nanoscale carriers for drugs, in order to bypass transporter proteins in cancer cells which efflux conventional therapeutics. These carriers include micelles, liposomes, gold nanoparticles, and a range of polymers, with a developing focus on materials which can respond to biological or external stimuli to release the drug payload once the carrier has reached its intracellular target.[14–18] Among these various stimuli, redox sensitive systems are particularly advantageous as there are a variety of redox gradients *in vivo*.[19] For triple negative breast cancer in particular, it has been demonstrated that the glutathione biosynthesis pathway and redox gradients are related to recurrence and poor prognostics and may be an important target for the treatment of the disease.[20–23] Accordingly, in this work, we have assessed the efficacy of a developed DTX-loaded redox-responsive formulation, assembled as micellar-like nanoparticles (MLNP)[23] and have compared these to analogous non-responsive DTX-loaded micellar-like nanoparticles, and free DTX in a 3D multi-cellular spheroids model. Here we show that the 3D model presents ABCG2/BCRP transporters, up-regulated at the mRNA and protein levels in comparison to 2D monolayers of the same TNBC cell line. Furthermore, the *in vitro* efficacy results indicate that the intrinsic MDR developed by the 3D multi-cellular spheroids model affects the efficacy of DTX but not the DTX-loaded MLNPs, with the redox-responsive cross-linked counterparts having the highest efficacy (Fig. 1).

2 Results and discussion

2.1. Development and optimisation of multicellular triple negative breast cancer spheroids

Triple negative breast cancer MDA-MB-231 cells were found to form centrally positioned spheroids in each well of ultra-low attachment (ULA) round bottom 96-well plates. After seeding the cells, the plate was centrifuged in order to encourage single spheroid formation and cell survival.[24] Gentle centrifugation was found to reduce cell loss, and viable spheroids were formed within 24 h by seeding from 1000 to 8000 cells per well. The spheroids were cultured for 72 h and the use of extracellular matrix enabled homogeneous and compact spheroids to be formed.[25]

The MDA-MB-231 TNBC cells formed spheroids varying from 209 μm (1000 cells) to 513 μm (8000 cells) in diameter with a standard deviation (SD) < 10 for the population of spheroids of different sizes (n = 6). In Fig. 2A is presented the phase contrast images of some of the spheroids from different number of cells after 72 hours of incubation. The correlation between the diameter of the spheroids and the initial number of cells seeded is represented as a scatter plot graph in Fig. 2B. As apparent from the data, triple negative breast cancer tumour spheroids exhibited size (diameter μm) increase over the three days duration of the incubation relative to the number of cells seeded. This correlation between the seeding concentration and proliferation capacity of MDA-MB-231 spheroids was similar to previous reports for these cell types.[26]

In addition to investigating growth patterns, the correlation between the number of cells seeded initially, viability and spheroids volume of cells within spheroids of various size were also assessed, as shown in Fig. 2C and D. The viability of the spheroids was evaluated using an ATP-based viability assay (CellTiter-Glo®).

As shown in Fig. 2C, the spheroids with various numbers of cells had viability increased according to the initial seeding density. The amount of the ATP measured by the ATP-based viability assay within the spheroids correlated nearly linearly (r = 0.99), with only the smallest (1000 cell) spheroids deviating slightly from the linearity.

The correlation between the spheroid volume (mm^3) and the cell viability reported by luminescence as a function of cytoplasmic ATP concentration of the spheroids is shown in Fig. 2D. These results indicate that for healthy spheroids, over the range of 200–500 μm in diameter, volume and also diameter correlated best with the number of viable cells within the MDA-MB-231 spheroids. It has been reported that for the larger spheroids, the core first becomes hypoxic and then necrotic as it has reduced access to nutrients and oxygen. In contrast, while the core of the spheroids is less populated, the periphery is a proliferating zone containing areas with a layer of densely packed cells.[27–30] These data support the correlation between the volume and number of cells seeded. We therefore chose for subsequent experiments a model with 4000 MDA-MB-231 cells per spheroid as optimum for proliferation rate, spheroid diameter and reproducibility.

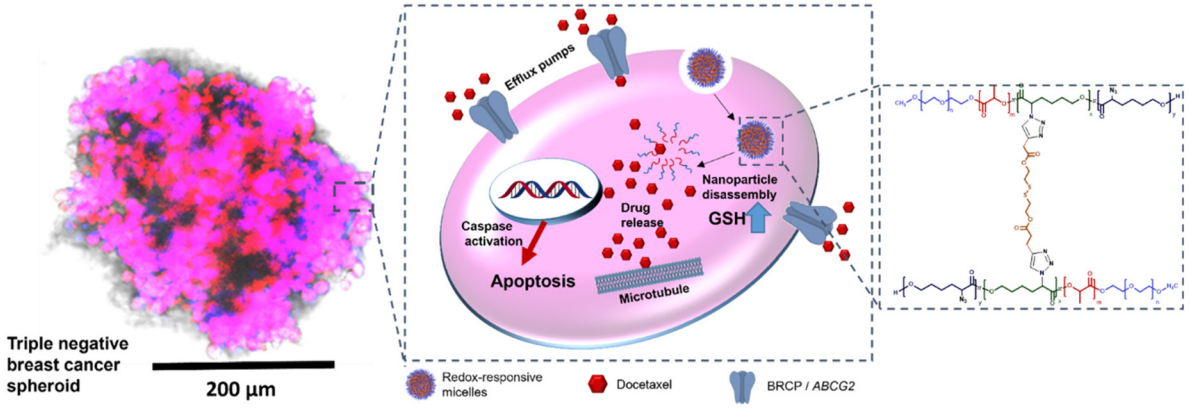

Fig. 1 Schematic illustration of the mode of action of redox-responsive micelles against triple negative breast cancer (TNBC) spheroids. On the left is a microscopy image of a spheroid of MDA-MB-231 cells with staining as follows: blue channel: showing nuclei stained with Hoechst, red channel: Cy5-labelled redox-responsive micelles. Spheroid showing superimposition of all channels – scale bar 200 µm. On the right hand side is the structure of the polymer used to form the micellar-like nanoparticles.

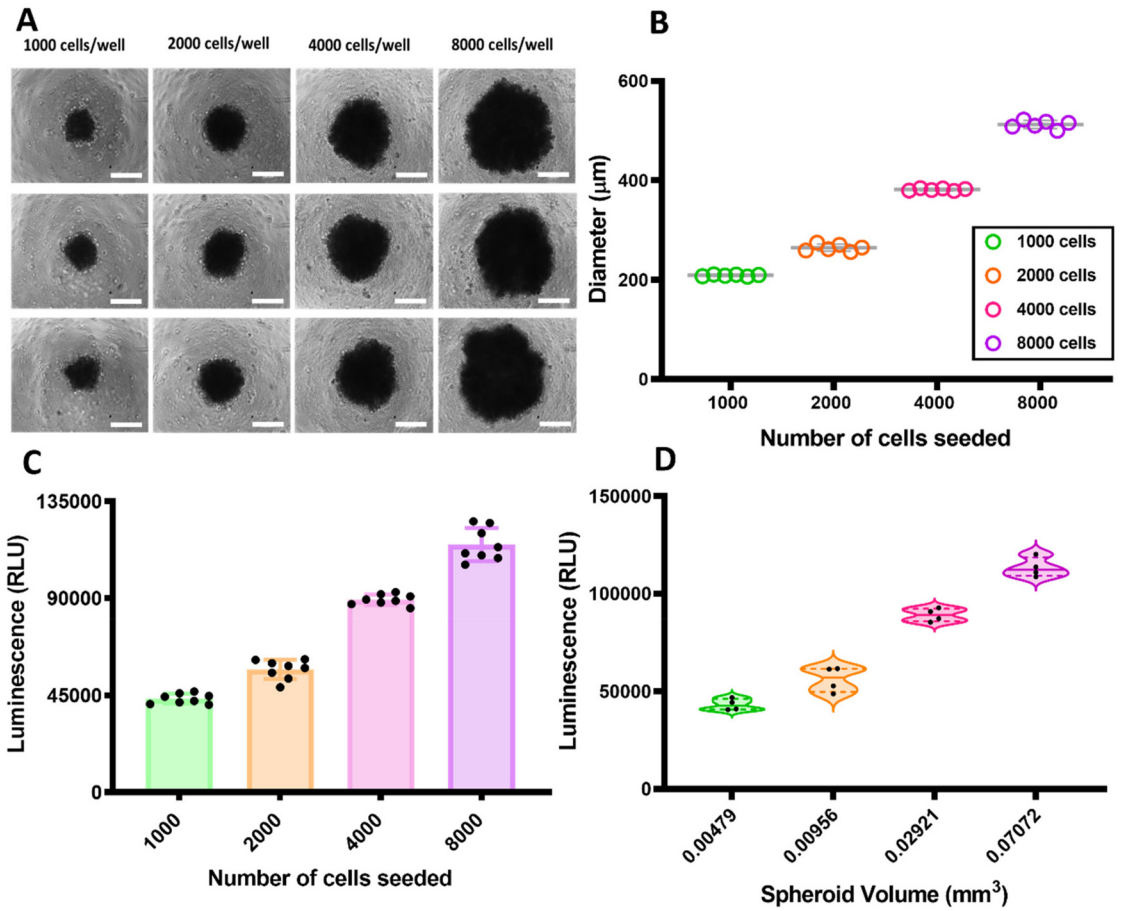

Fig. 2 (A) TNBC spheroids of different diameters relative to the number of cells seeded. The images were obtained from a Phase Contrast Microscope (Imstar) and the images of the spheroids were taken on day 3 of culture. Scale bar 200 µm. (B) Scatter plot graph showing the relation between the number of cells seeded for obtaining the multicellular spheroids with the diameter of each individual spheroid (n = 6). (C) CellTiter-Glo® 3D Cell Viability assay was performed within different days to investigate the viability of the spheroids formed 3 days after seeding. Scatter plot graph with bar (including all points n = 8) showing the initial number of cells seeded *versus* the luminescence referent to the viability of spheroids. (D) CellTiter-Glo® 3D Cell Viability assay was performed to investigate the relation between bioluminescence and spheroid volume. Violin plots (n = 4) showing the volume (mm^3) of the spheroids *versus* the luminescence.

The 72 hour incubation for the 3D spheroids formation was selected to balance spheroid development with model reproducibility within a practical timeframe. The observed correlation between spheroid size and the number of cells seeded was found to be consistent with previous studies[27–30] indicating reliable growth patterns. Although more extended growth periods are employed in some studies, shorter incubation periods offer advantages, such as accelerated experimental timelines and potentially fewer environmental variables affecting spheroid integrity. It is acknowledged that rapidly developed spheroids may exhibit different cell viability and proliferation dynamics compared to those grown over longer durations. To address this aspect, an ATP-based viability assessment was conducted within the 72 hour window, revealing a near-linear correlation between spheroid volume and cell viability. This finding suggests that even within a shorter incubation period, the spheroids adequately represent cellular behaviour. Potential limitations, such as the risk of hypoxia and necrosis in larger spheroids, were also considered, and a model incorporating 4000 cells per spheroid was selected. This configuration was deemed optimal for maintaining healthy proliferation rates and providing reliable and reproducible data for subsequent experiments. While extended growth periods might offer deeper insights into longer-term spheroid development, the approach taken prioritizes rapid and consistent results, effectively balancing practicality with model fidelity.

2.2. Effects of blank (non-drug-loaded) MLNPs in 2D monolayers and 3D spheroids of MDA-MB-231 cells

All procedures regarding synthesis of polymers, linkers, further functionalisation and characterisation along with the preparation of all formulations (blank and DTX-loaded formulations) were reported in our previous work.[23] The cytotoxicity of empty crosslinked and un-crosslinked MLNPs in 2D monolayers and 3D spheroids was assessed using a luminescence-based cell metabolic activity assay as a proxy of viability. Cell monolayers and spheroids were exposed to different concentrations of micelles for 24 h and results demonstrated that both crosslinked and un-crosslinked MLNPs did not show any *in vitro* cytotoxicity under the tested conditions. Transport and cell internalisation of Cy5-labelled micelles was also assessed in 3D multicellular tumour spheroids of MDA-MB-231 cells. 4000 cells were seeded into a ULA 96 well-plate and the entire experiment, including the spheroids imaging, was carried out in the ULA plate. After seeding the cells, the spheroids were formed within 3 days and they were exposed to 50 μg mL^{-1} of Cy5-labelled crosslinked and un-crosslinked micelles and were incubated for 5 h. Spheroids were washed carefully and fixed.

As apparent from Fig. 3, the metabolic activity of the cells in the presence of micelles was always more than 85% compared to negative controls. The viability results were similar to those obtained for the 2D monolayers treated with empty crosslinked and un-crosslinked MLNPs. Microscopy data (Fig. 3C–J) indicated that Cy5-micelles were clearly internalised by the MDA-MB-231 cells in the spheroids, in accord with data from transport studies in 2D monolayers (Fig. S1†).

2.3. Effects of DTX-loaded crosslinked and un-crosslinked MLNPs and free-DTX in 2D monolayers and 3D spheroids of MDA-MB-231 cells

Several methods were employed to assess the efficacy of the various formulations in 2D monolayers and 3D spheroids as shown below.

2.3.1. Efficacy assessment by CellTiter-Glo® 3D Cell Viability Assay. Initially, an ATP based viability assay (CellTiter-Glo® 3D Assay) for quantifying the ATP levels of the treated monolayers and spheroids was employed. As shown in Fig. 4, both 2D monolayers and 3D spheroids were treated with different concentrations of crosslinked and un-crosslinked MLNPs and free DTX. The concentration of DTX was kept constant for the purpose of comparisons between the different treatments.

As seen in Fig. 4B, generally, the DTX-loaded MLNPs and also the free DTX decreased the viability of the spheroids, as determined by the amount of the ATP measured from the lysed cells within spheroids. At 7 μg mL^{-1} of DTX, no significant differences were observed among the treatments compared to the negative control or untreated spheroids. However, as the tested concentrations of drug increase, the differences between the effects of the treatments on the spheroids viability became evident. Specifically, spheroids treated with DTX-loaded crosslinked MLNPs had the most pronounced effect on the MDA-MB-231 spheroids compared to the other treatments. Compared to the negative control and free DTX, the treatment of the spheroids with DTX-loaded crosslinked MLNPs (concentration range of 10–40 μg mL^{-1}) promoted a marked decrease of the spheroids' viability having significant differences ($p < 0.0001$) as verified by two-way ANOVA with Tukey's *post hoc* test.

The DTX-loaded un-crosslinked micelles also decreased the viability of the spheroids compared to the untreated spheroids and had better efficacy than the free DTX with significant differences among the treatments within the concentration range of 10–40 μg mL^{-1} of DTX. Data in Fig. 4B also show that the free DTX decreased the viability of the spheroids compared to the untreated cells from a concentration of 15 μg mL^{-1} but not at 7 to 10 μg mL^{-1} of free DTX.

Regarding the differences in 2D monolayers and 3D cell cultures (Fig. 4A and B) it was apparent that the DTX-loaded formulation and free DTX had decreased efficacy in 3D compared to 2D cultures. Thus, the tumour spheroids appear to be more resistant to all the treatments in comparison with 2D monolayers of MDA-MB-231. For all the treatments, but especially for the free DTX, cytotoxicity was less in multicellular spheroids than on the 2D monolayers. This effect can be correlated with the mechanisms of resistance associated with properties of the spheroid microenvironment, as previously discussed.

For further confirmation of the efficacy of DTX-loaded MLNPs compared to free DTX in 3D cell culture, cell death was assessed by using additional and experimentally orthogonal methods, as shown below.

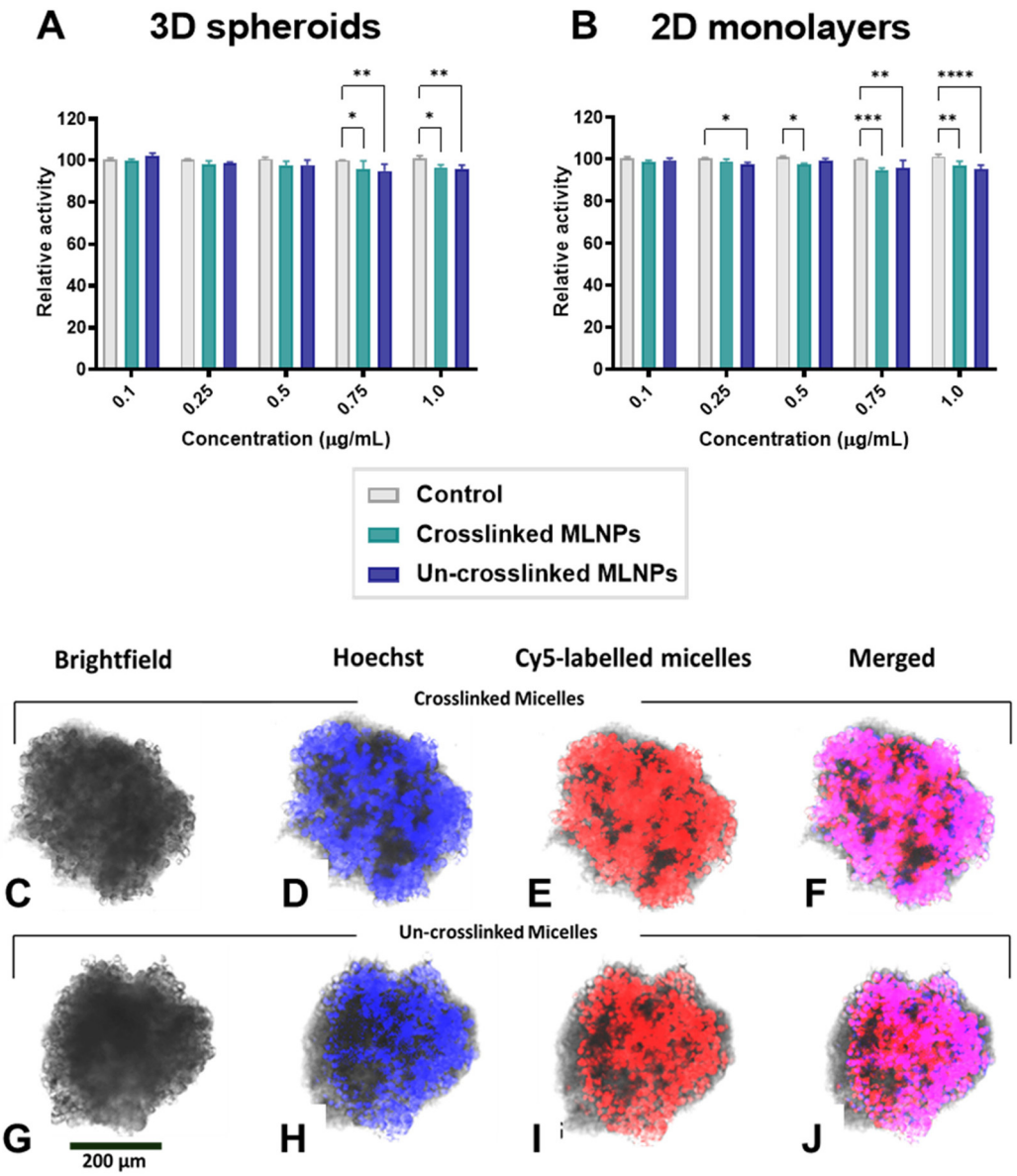

Fig. 3 (A and B) MDA-MB-231 cells were seeded as monolayers and spheroids and both were treated with empty crosslinked and un-crosslinked MLNPs for 24 hours, and then assayed with the CellTiter-Glo® 3D Reagent. Luminescence was recorded at 30 minutes. Error bars show standard deviation (n = 5). (*p < 0.05, **p < 0.01, two-way ANOVA with Tukey's post-test). (C–J) Transport and internalisation of Cy5-labelled crosslinked and un-crosslinked micelles in 3D multicellular spheroids of MDA-MB-231 cells. Spheroids were allowed to grow for 3 days and then treated with 50 μg mL^{-1} of Cy5-labelled micelles for 5 h. Brightfield showing the multicellular spheroids (C and G). Blue channel: showing nuclei stained with Hoechst (D and H). Red channel: Cy5-labelled crosslinked micelles (E) and Cy5-labelled un-crosslinked micelles (I). Merged: superimposition of all channels (F and J) – Scale bar 200 μm.

2.3.2. Evaluation of apoptosis in 3D spheroid culture of MDA-MB-231 cells following treatment with MLNPs. Spheroids were obtained as described previously and cells were treated with free DTX, DTX-loaded crosslinked and un-crosslinked MLNPs for 24 h. As before, the concentration of DTX as a free drug and loaded in the formulations, was kept constant for the purpose of comparisons among the different treatments. The single cell suspensions were pooled together and stained with annexin-V FITC/PI. Cells were then classified as viable, apoptotic (early and late stages), and dead cells, using flow cytometry, as shown in Fig. 5. Controls were prepared to observe the basal level of apoptosis/necrosis in the tumour spheroids (stained spheroids), and also the auto-fluorescence of spheroids (unstained spheroids). As seen in Fig. 5B, the unlabelled cells had a low basal fluorescence, whereas the annexin-V/PI treated spheroids (control) showed a relatively high number of apoptotic cells (late and early stages).

As seen in Fig. 5A and B, cells exposed to crosslinked MLNPs were more apoptotic (considering early and late apoptosis) to a level of 39%, followed by un-crosslinked MLNPs (35%). The free DTX exhibited 26% of apoptotic cells, which was the same as for the untreated spheroids (basal level of

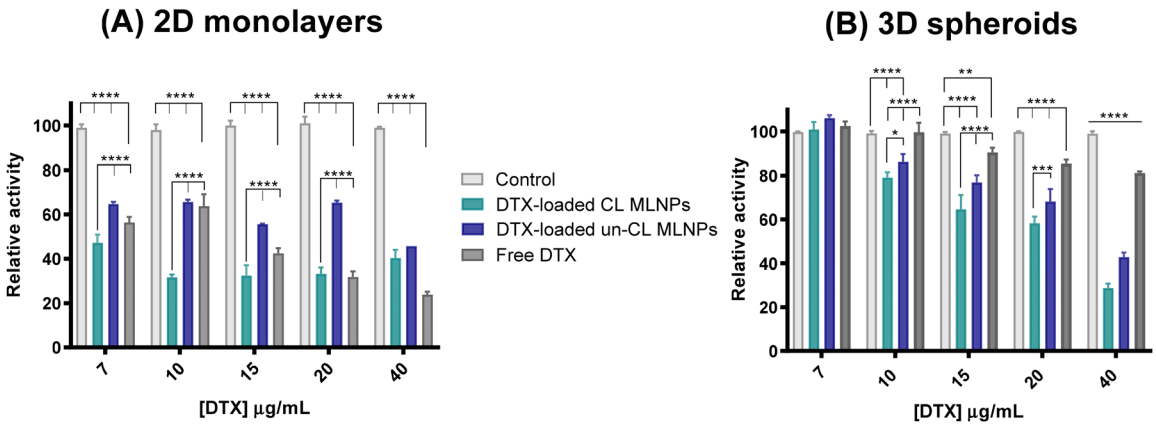

Fig. 4 CellTiter-Glo® 3D Cell Viability assay: ATP-based viability test for 2D monolayers (A) and 3D spheroids (B) – (A) MDA-MB-231 cells were seeded at a density of 5 x 10^3 cells per well and incubated at 37 °C and 5% of CO_2 for 24 h and treated with DTX-loaded micelles and free DTX for 24 hours, and assayed with the CellTiter-Glo® 3D Reagent. (B) For 3D spheroids MDA-MB-231 cells were seeded as follows: 4000 in ULA plates were grown for 3 days, spheroids were treated with DTX-loaded micelles and free DTX for 24 hours, and then assayed with the CellTiter-Glo® 3D Reagent. Luminescence was recorded at 30 minutes. DTX-loaded crosslinked micelles were more cytotoxic in comparison to the un-crosslinked micelles and free DTX was less toxic than the other treatments. Error bars show standard deviation (n = 4). (*p < 0.05, **p < 0.01, ****p < 0.0001 two-way ANOVA with Tukey's *post hoc* test).

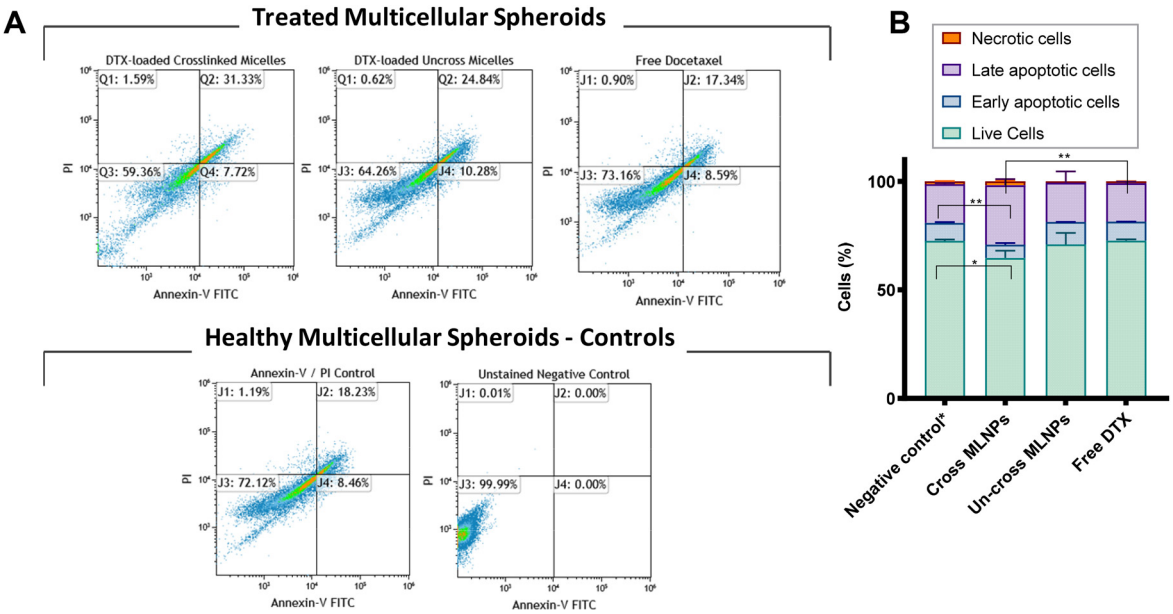

Fig. 5 (A) Controls in the panels showing unstained dissociated MDA-MB-231 tumour spheroids and spheroids negative controls for annexin-V FITC and PI. Samples were analysed by flow cytometry and as shown in each panel, Q3 shows live cells which are negative for both annexin-V and PI, whereas Q4 shows cells that are negative for PI but positive for annexin *i.e.* in the early stage of apoptosis. Cells in the late stage of apoptosis are in Q2. Q1 shows dead cells which are positive for PI and negative for annexin. (B) Graph shows the proportion (%) of different cell populations after treatment with DTX-loaded crosslinked, un-crosslinked MLNPs and free DTX using annexin-V/PI assay. At 7 μg mL^{-1} of DTX both DTX-crosslinked (especially) and un-crosslinked MLNPs induced apoptosis in the TNBC spheroids whereas the free DTX did not induce cells to apoptosis. As noticeable, the negative control (untreated spheroids) and the free DTX (treated spheroids) had the same number of apoptotic cells, considering both early and late apoptosis. Error bars show standard deviation (n = 3). (*p < 0.05, **p < 0.01, ****p < 0.0001 two-way ANOVA with Tukey's *post hoc* test).

apoptotic cells in the multicellular tumour spheroids). Therefore, DTX-loaded crosslinked MLNPs were of greater efficacy in inducing apoptosis in MDA-MB-231 spheroids than the other treatments, namely DTX-un-crosslinked MLNPs and free DTX. The free DTX at the concentration of 7 μg mL^{-1} was not able to induce apoptosis in the multicellular tumour spheroids.

2.3.3. Evaluation of caspase 3/7 activity in 3D spheroid culture of MDA-MB-231 cells following treatment with MLNPs. In order to corroborate these results with those of the previous

efficacy assays, the caspase (3/7) activity of the treated multicellular spheroids was also assessed. The activation of caspase enzymes, which are cysteine-aspartic acid-specific proteases, is a feature of the early stages of apoptosis. During apoptosis, caspase-3 and caspase-7 proteins are activated and able to cleave the caspase 3/7 recognition sequence encoded in the DEVD peptide from the reagent. Cleavage of the recognition sequence, and binding of DNA by the reagent, results in labelling of apoptotic cells with a fluorogenic signal, and when combined with an appropriate dye, it is possible to distinguish between live, apoptotic, and necrotic cell populations in this assay, as shown in Fig. 6A.

It is clear from Fig. 6A and B that spheroids exposed to crosslinked MLNPs had a higher amount of caspase 3/7 active cells, and therefore cells were more apoptotic to a level of 12%, followed by un-crosslinked MLNPs (8%). Cells treated with free DTX showed 5% of caspase 3/7 activity or apoptosis which was the same amount obtained from the untreated spheroids (basal level of apoptotic cells by caspase 3/7 and SYTOX™ red assay in multicellular tumour spheroids). Therefore, these results corroborate with the previous findings regarding the efficacy of the DTX-loaded MLNPs compared to the free DTX assessed by ATP luminescence and annexin-V/PI assays.

There are some interesting differences in the results of the apoptosis assays in 3D cultures of triple negative breast cancer cells compared to those observed in 2D monolayers, as reported previously.[23] Although, the formulations of MLNPs and the amount of drug were kept constant in both assessments, the number of apoptotic and necrotic cells from multicellular tumour spheroids is markedly higher than for the monolayers of MDA-MB-231 cells (Fig. 5 and 6 and S3†). This elevated number of apoptotic/necrotic cells found in the untreated spheroids can be explained due to the chemical gradients in terms of oxygen, nutrients and necrotic areas according to the size of the spheroids. This is, as expected, in contrast to the case of conventional 2D cell culture, in which the cells are grown as monolayers in a manner distinct from that found in tumours *in vivo*.

There are also differences in the efficacy as assessed by apoptosis assays of the DTX-loaded MLNPs and free DTX in 3D spheroids compared to those we reported in 2D monolayers.[23] Thus, when assessing the efficacy by an ATP-based viability test (Fig. 4), in general, the spheroids were less sensitive to the treatment with DTX-loaded MLNPs and free DTX in comparison to 2D monolayers. In case of the efficacy of free DTX, as seen in Fig. 4–6 the effects of culturing the cells in 3D cell culture were noticeable. Free DTX did not induce any cells to apoptosis/necrosis in the 3D cultures, whereas in 2D monolayers the results were distinct, *i.e.* the treatment with free DTX induced about 23% of the cells to apoptosis (early and late

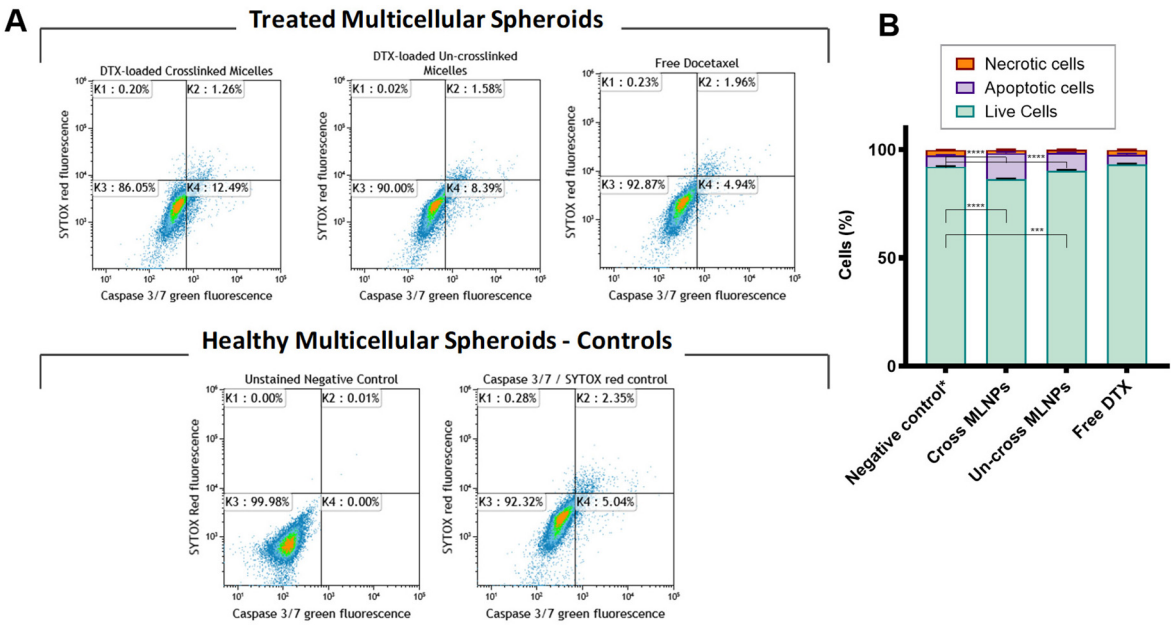

Fig. 6 (A) Caspase 3/7 Sytox assay assessed for MDA-MB-231 tumour spheroids. Cells were seeded as follows: 4000 in ULA plates were grown for 3 days after the treatment spheroids were carefully dissociated by repeated pipetting. The resultant single cell suspensions from six wells per condition were pooled together. MDA-MB-231 triple negative breast cancer spheroids were treated with DTX-loaded crosslinked and un-crosslinked MLNPs and free DTX for 24 h. Controls in the panels showing unstained MDA-MB-231 breast cancer dissociated spheroids and cells stained CellEvent caspase 3/7 and Sytox (stained control). Samples were labeled with the CellEvent caspase 3/7 and Sytox red and analysed by flow cytometry. As shown in each panel, K3 shows viable cells which are negative for CellEvent caspase 3/7 and Sytox red, whereas K4 shows apoptotic cells which are positive for CellEvent caspase 3/7. Necrotic cells (K2) are positive for Sytox red and CellEvent caspase 3/7. (B) Graph shows the proportion (%) of cells with caspase-3/7 activation after treatment with DTX-loaded crosslinked, un-crosslinked MLNPs and free DTX using caspase 3/7 Sytox assay. At 7 μg mL^{-1} of DTX both DTX-crosslinked (especially) and un-crosslinked MLNPs had a higher number of caspase 3/7 activation in comparison with the free DTX. This data corroborates with the previous annexin-V/PI assay. Error bars show standard deviation (n = 3). (*p < 0.05, **p < 0.01, ****p < 0.0001 two-way ANOVA with Tukey's *post-hoc* test).

stages) and about 7% of the cell population was necrotic. In addition, the effect of the treatment with DTX-loaded MLNPs and free DTX in 2D monolayers led to significantly fewer viable cells in comparison to 3D spheroids. Moreover, spheroids treated with DTX-loaded MLNPs and free DTX had decreased activity of the apoptotic biomarkers caspase 3 and 7 (Fig. 6). Thus, the efficacy results from the DTX-loaded MLNPs and free DTX obtained from the caspase 3/7 and Sytox assay by flow cytometry corroborated with the results of the efficacy tests found by assessing the ATP levels and by the annexin-V/PI apoptosis assays.

Overall, comparing the sensitivity of both models (2D and 3D cultures) to the DTX-loaded MLNPs and free DTX, these data indicate that 3D cell culture model was more resistant to all treatments. In addition, the results suggest that 3D tumour spheroids were chemoresistant to DTX as the spheroids did not have any sensitivity to free DTX when assessed by apoptosis biomarkers and also, presented higher viability, especially after the treatment with free DTX (measured by intracellular ATP levels). On the other hand, the DTX-loaded MLNPs, and in particular the DTX-loaded crosslinked MLNPs were the most potent, with an apparent ability to overcome the resistance mechanism that affected the free DTX. Thus, to test these hypotheses regarding the chemoresistance of MDA-MB-231 multicellular spheroids, assessment of the expression of genes and protein related to the ATP-binding cassette (ABC) transporters, was performed.

2.4. Assessing gene expression of ABC transporters in 3D spheroids and 2D monolayers by quantitative PCR analysis, western blot and immunofluorescence

One of the most important mechanisms in conferring MDR is the overexpression of ATP-binding cassette (ABC) transporters in cancer cells. Some of these proteins can decrease the intracellular drug concentration by pumping a variety of drugs out of the cancer cells. We therefore assessed the effects of culturing cells in 3D compared to 2D cultures in terms of the expression of some ABC transporters related to MDR. Initially, the RNA levels of the genes ABCB1/MDR1 and ABCG2/BCRP, which encode respectively the P-glycoprotein and human breast cancer resistance protein (BCRP) were assessed by RT-qPCR. The results are presented in Fig. 7A.

The ABCG2/BCRP expression at mRNA level was increased 76-fold in the MDA-MB-231 tumour spheroids when compared to conventional 2D monolayers. Regarding the ABCB1/MDR1 gene, we did not find any expression in either MDA-MB-231 tumour spheroids or the 2D monolayers. Following the results obtained from the RT-qPCR analyses related to the expression of ABCG2 genes, immunofluorescence and western blot assays were also performed in order to assess the ABCG2/MDRP protein levels in both 2D monolayers and 3D spheroids of MDA-MB-231 cells. The results are presented in Fig. 7C and D. Through immunofluorescence assays using confocal microscopy, it was apparent that PE-labelled ABCG2 monoclonal antibody was found only in the spheroids but not in the 2D monolayers of the same TNBC cell line. In order to confirm the results, the expression of ABCG2/MDRP was also investigated by western blot assays (Fig. 7D). Again, from the results it was noticeable that the ABCG2/BCRP protein was expressed in 3D spheroids but not in 2D monolayers. The results in Fig. 7 showing ABCG2 mRNA and protein expressions were thus complementary and in agreement with each other.

The ABCG2/BCRP gene is a member of the ATP-binding cassette (ABC) transporters and its encoded protein, named breast cancer resistance protein, has emerged as an important multidrug resistance protein. Some of the natural functions of BCRP are related to the protection of the organism from xenobiotics as the protein is expressed in a subset of progenitor/stem cells in all of the main tissues of the body.[31] However, ABCG2/BCRP has a high efflux capacity as a transporter, thus when overexpressed in cancer cells it can recognise and prevent diverse drugs from entering cells. The classes of anticancer drugs that have been found to be substrates of ABCG2/BCRP includes methotrexate, mitoxantrone, camptothecin-derived and indolocarbazole topoisomerase I inhibitors, flavopiridol, and quinazoline ErbB1 inhibitors. A variety of anthracyclines were also found to be effluxed by BCRP, in part dependent on the presence of a ABCG2/BCRP mutation at codon 482.[32–34] Regarding taxanes, although docetaxel is not normally regarded as a BCRP substrate, it has been found that up-regulated phosphorylated ABCG2/BCRP enhanced resistance to DTX in a prostate cancer cell line.[35] In addition, it has been shown that ABCG2/BCRP expressed in LNCaP, PC3, and HEK293 cells were able to efflux DTX and these cells were significantly more resistant to DTX than control cells.[36] It has been also found the effect was specific to ABCG2/BCRP as an inhibitor was used which impeded resistance to DTX.[36] We suggest therefore that the enhanced resistance of the TNBC 3D spheroids when compared to the same cells grown in monolayers can be attributed to the increased expression of the gene ABCG2 and expression of the corresponding protein. To the best of our knowledge, this is the first study which shows that growing MDA-MB-231 cells as 3D multicellular spheroids promotes an up-regulation and expression of respectively ABCG2/BCRP gene and protein related to MDR compared to 2D monolayers.

It has been reported that pancreatic and melanoma cancer cell lines grown in 3D culture had increased expression of some resistance genes which led to augmented drug resistance in 3D culture compared to 2D culture.[37,38] Other reported mechanisms of resistance that can be corroborated to the lack of sensitivity to DTX in 3D cell culture include the postulates that cells on the outside of spheroids can protect the cells on the inside from drug penetration.[39] However, the reduction-responsive crosslinked MLNPs containing DTX showed enhanced efficacy against TNBC tumour spheroids in terms of total volume reduction,[23] suggesting that the micellar-like carriers overcame, or bypassed, the DTX-resistance mechanism developed in the MDA-MB-231 TNBC multicellular spheroids. We suggest that because the micelles enter cells *via* endocytosis routes rather than diffusion across the cell membranes, the

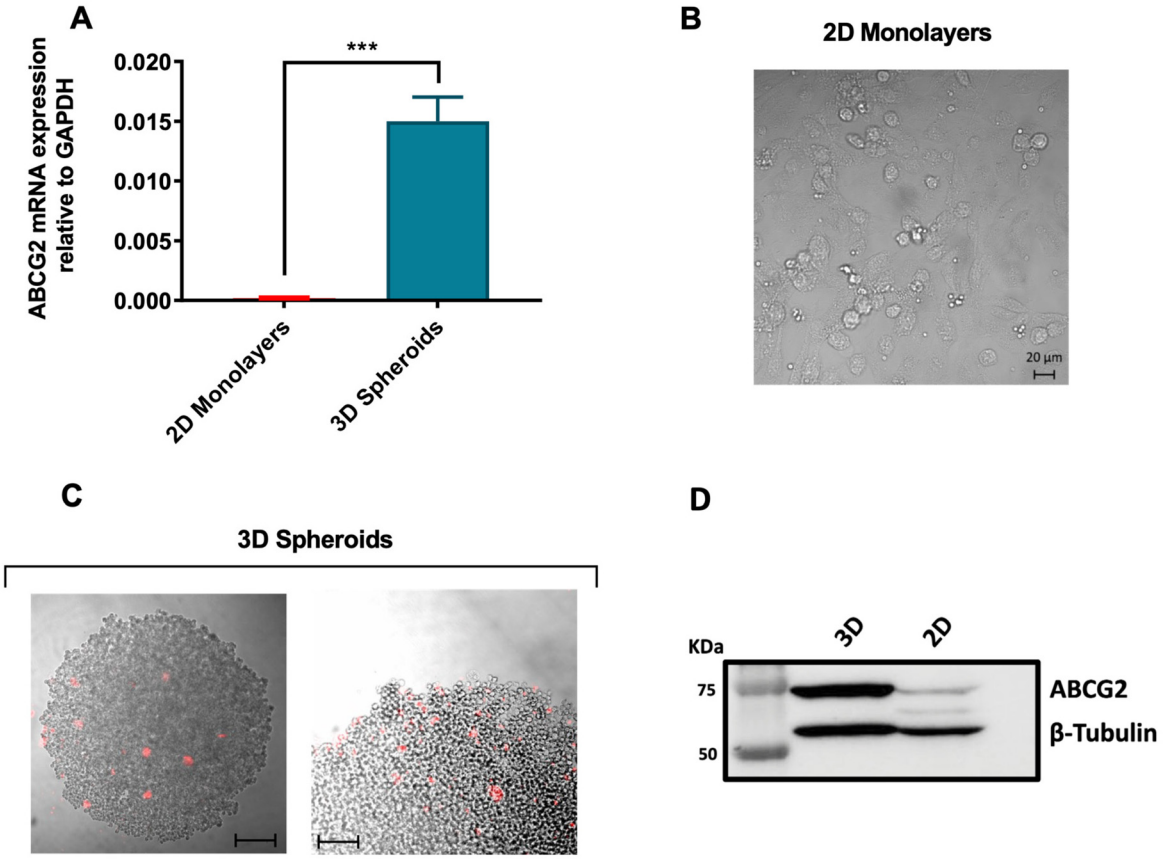

Fig. 7 (A) Expression of ABCG2/BCRP gene in MDA-MB-231 cells (2D and 3D cell culture) assessed by RT-qPCR – The expression of ABCG2 at mRNA levels was 76-fold higher in 3D spheroids in comparison with 2D monolayers (n = 3; t-test, $P < 0.05$). (B and C) Immunofluorescence assays in 2D monolayers and 3D spheroids of MDA-MB-231 cells for assessing the expression of ABCG2/BCRP using PE-labelled CD338 (ABCG2) monoclonal antibody – 2D monolayers did not show apparent expression of ABCG2/BCRP. (D) Western blot showing expression of ABCG2/BCRP in 2D monolayers and 3D spheroids of MDA-MB-231 cells. β-Tubulin was used as a reference protein.

carriers avoided the ABC transporters which otherwise exported free DTX. In addition, the enhanced resistance in 3D spheroids could be linked to the up-regulation of ABCG2 at RNA levels and higher expression of ABCG2/MDRP in MDA-MB-231 spheroids in comparison to 2D monolayers, thus accentuating differences between drug entering/leaving cells *via* a carrier or *via* membrane-transporters.

The utilization of a 3D spheroid culture system in this study provides a more accurate representation of the *in vivo* microenvironment compared to traditional 2D cultures. This model facilitates the replication of crucial physiological conditions, such as cell–cell interactions and nutrient gradients, which are essential for predicting cellular responses. Previous studies have demonstrated that such 3D models correlate closely with *in vivo* outcomes. For instance, where the responses observed in developed multicellular gastric cancer spheroids replicated the characteristics of the original carcinoma and the therapeutic efficacy seen in xenografts in immunodeficient mice.[40,41] In addition, studies have demonstrated that drug responses observed in TNBC 3D spheroid models correlate with outcomes in patient-derived xenografts (PDX) and murine models, particularly in terms of multi-drug resistance (MDR) mechanisms and upregulation of ABCG2/BCRP expression.[42,43] The ABCG2/BCRP transporter, which was found to be upregulated in TNBC 3D spheroid model in this work, has also been associated with chemoresistance in patient tumours and linked to poor treatment responses in clinical settings.[44,45] These findings underscore the translational relevance of the model used in this work, supporting its utility as a preclinical tool for studying TNBC drug resistance and evaluating novel therapeutic strategies prior to *in vivo* validation.

3. Conclusions

In this work, we assessed the efficacy of DTX-loaded crosslinked, un-crosslinked MLNPs, and free DTX, in 2D and 3D cell culture models of triple negative breast cancer. Taken together, the results of the efficacy assays demonstrate that DTX-loaded crosslinked MLNPs had the best efficacy against TNBC spheroids compared to control (un-crosslinked MLNPs) and free DTX. Compared to their un-crosslinked counterparts,

the crosslinked MLNPs exhibit higher cytotoxic effects, likely because they enhance the delivery of DTX within cells. Furthermore, the presence of a redox-crosslinker in the core of these stimuli-responsive particles may lead to increased DTX release, triggered by the elevated GSH levels in triple-negative and breast cancer cells. The efficacy data of DTX-loaded MLNPs and free DTX indicate that the biological evidence shown by 2D and 3D cell cultures are markedly different, as 3D tumour spheroids exhibited higher innate resistance, especially to the free docetaxel. Thus, this work supports the premise that 3D tumour models are indeed relevant to mimic certain *in vivo* conditions, which allows a more realistic *in vitro* evaluation of nanomedicines. In addition, since the DTX-loaded redox-responsive crosslinked MLNPs demonstrated efficacy in complex multicellular tumour mimics, we conclude that the MLNP carriers are promising candidates for further use in *in vivo* efficacy assessments.

4. Materials and methods

4.1. Cell lines and culture

Triple negative breast cancer cell line MDA-MB-231 was acquired from the American Type Culture Collection (Manassas, VA). The cells were maintained in Dulbecco's modified Eagle's medium (DMEM, Lonza, Inc), supplemented with 10% (v/v) FBS and 1% penicillin/streptomycin and incubated at 37 °C in 5% CO_2.

4.2. Development and optimisation of multicellular triple negative breast cancer spheroids

TNBC tumour spheroids were obtained by using ultra-low attachment (ULA) 96-well round bottom plates which are commercially available plates pre-coated with a hydrophilic, neutrally charged hydrogel. The hydrogel prevents specific and non-specific immobilisation and triggers the formation of a single spheroid per well. Using these plates, spheroids of different size were formed in DMEM media using single-cell suspensions of MDA-MB-231 TNBC cells with a constant volume of 150 μL and number of cells ranging from 1000 to 8000 cells per well. For optimal spheroid formation Matrigel was added in each well with the final concentration of 2%. The plates were centrifuged at 300*g* for 3 minutes after seeding to bring the cells closer together and aid in the formation of a single spheroid. Spheroids were cultured for 3 days before final analysis or treatment.

4.3. Spheroid viability assessment

Images of the spheroids were taken daily for growth determination experiments using a phase-contrast microscope with a 10× objective. On day 4, a cytotoxicity assay (CellTiter-Glo® 3D Cell Viability Assay) for checking the viability of the spheroids was performed.

4.4. CellTiter-Glo® 3D cell viability assay

The viability of the spheroids was assessed by the CellTiter-Glo® 3D Cell Viability Assay Promega assay. MDA-MB-231 cells were seeded into a ULA 96 well-plate at different densities (1000, 2000, 4000 and 8000 cells per well). The plate was centrifuged at 300*g* for 3 minutes to bring the cells closer together and to facilitate the formation of a single spheroid per well. The cells were then incubated at 37 °C and 5% of CO_2 for 72 h. 100 μg mL^{-1} of CellTiter-Glo 3D reagent was then added to each well and the contents were vigorously shaken for 15 minutes to induce cell lysis. The plate was incubated at room temperature for an additional 25 minutes to stabilise the luminescent signal. Luminescence was measured using a GloMax 96 Microplate Luminometer (Promega).

4.5. Assessing gene expression in 3D spheroids by reverse transcriptase and quantitative PCR analysis

RT-PCR analysis was performed to assess the expression of two genes related to MDR in breast cancer (ABCB1/MDR1, ABCG2/BCRP) in 2D monolayers and 3D spheroids. Primers sequences were: ABCB1: forward primer, 5′-CCCATCATTGCAATAG CAGG-3′, reverse primer, 5′-GTTCAAACTTCTGCTCCTGA-3′. ABCG2: forward primer, 5′-TGCAACATGTACTGGCGAAGA-3′, reverse primer, 5′-TCTTCCACAAGCCCCAGG-3′.

For the preparation of tumour spheroids, MDA-MB-231 cells (4000) were seeded into a ULA 96 well-plate. The plate was centrifuged at 300*g* for 3 minutes to bring the cells closer together and to facilitate the formation of a single spheroid per well. The cells were then incubated at 37 °C and 5% of CO_2 for 3 days. On day 4, spheroids were pooled together then dissociated using TrypLE. Cell suspension was centrifuged and washed with PBS.

Total RNA was extracted with RNeasy Mini Kit (Qiagen, Hilden, Germany) according to manufacturer's instructions. Reverse transcription PCR (RT-PCR) was carried out with 500 ng of total RNA using QuantiTect Reverse Transcription Kit (Qiagen). Genomic DNA elimination was carried out twice, during RNA extraction and before the complementary DNA (cDNA) synthesis. RNA concentration and integrity were evaluated using an Agilent's 2100 Bioanalyzer. Following cDNA conversion, real time quantitative PCR (RT-qPCR) reactions were performed in 96-well white-walled plates using 2× Brilliant II SYBR® Green QPCR Master Mix (Agilent). Glyceraldehyde-3-phosphate dehydrogenase (GAPDH) was used as a reference control and ΔΔCq method was used to calculate relative gene expression.

4.6. Assessing the levels of ABCG2/BCRP protein using immunofluorescence by confocal microscopy

4.6.1. Preparation of the polymers and formulations. The procedures for the synthesis of the polymers and preparation of the formulations used in work, as well as the characterisation data are shown elsewhere.[29]

4.6.2. Cytotoxicity of the blank MLNPs. The cytotoxicity of the blank crosslinked and un-crosslinked MLNPs was assessed using CellTiter-Glo® 3D Cell Viability Assay in 3D spheroids and 2D monolayers of MDA-MB-231 cells. 2D Monolayers were obtained by seeding MDA-MB-231 into a 96 well-plate at a density of 5×10^3 cells per well and incubated at 37 °C and 5% of CO_2 for 24 h. Spheroids were obtained as previously

described. Afterwards, cells and spheroids were exposed to different concentrations of empty crosslinked and un-crosslinked MLNPs (100, 250, 500, 750 and 1000 μg mL^{-1}) for 24 hours. Controls containing only medium and cells were also prepared. MLNPs were diluted using complete medium. After the incubation period 100 μL of CellTiter-Glo 3D reagent was then added to each well and the procedure for assessing the viability was the same as previously described.

4.7. Efficacy of DTX-loaded crosslinked and un-crosslinked MLNPs and free-DTX in TNBC tumour spheroids

4.7.1. Luminescent cell viability assay – ATP measurements. MDA-MB-231 cells were seeded into a ULA microplate at a density of 4000 per well and the spheroids were formed using the same procedure as shown in the previous sections. The spheroids were then exposed to different concentrations (7, 10, 15 and 20 μg mL^{-1}) of DTX-loaded crosslinked, un-crosslinked MLNPs and free DTX (solubilised in DMSO), where the mentioned concentrations refer to the concentration of DTX in each formulation and as a free drug, for ensuring the results would be comparable. The final concentration of DMSO in the cells treated with DTX was less than 0.5%. The spheroids were then incubated for 24 h at 37 °C in 5% CO_2. Afterwards, 100 μL of CellTiter-Glo 3D reagent was then added to each well and the procedure for assessing the viability was the same as previously described.

4.8. Apoptosis assays

4.8.1. Annexin-V/PI assay. MDA-MB-231 cells were seeded into a ULA microplate at a density of 4000 per well and the spheroids were formed using the same procedure as shown previously. Cell culture medium was replaced with the medium containing free DTX, DTX-loaded crosslinked or un-crosslinked MLNPs at concentration of 7 μg mL^{-1} (of DTX) or medium in the absence of MLNPs (controls) and the spheroids were incubated for 24 h at 37 °C in 5% CO_2. After the incubation period, supernatants were collected and the spheroids were dissociated using TrypLE. The resultant single cell suspensions from six wells per condition/treatment were pooled together in a microcentrifuge tube and cells were centrifuged and washed with PBS 3 times. Afterwards, cells were resuspended in 100 μL of 1× annexin-binding buffer and 2.5 μL annexin-V FITC (Thermo Scientific) and 1 μL of 100 μg mL^{-1} PI solutions were added. Two negative controls were prepared, whereas one with the cells left untreated and unstained, while the other control was also obtained with untreated cells however, the cells were stained with annexin-V and PI, respectively. Single cell suspensions were then incubated in the dark for 15 min and then 400 μL of 1× annexin-binding buffer was added. Samples were immediately analysed using a Beckman Coulter FC 500 flow cytometer. Kaluza 1.5 software was used for the data analysis.

4.9. Detection of caspase-3/7 to distinguish between live, apoptotic and necrotic cell populations

As previously described for annexin-V/PI assay, MDA-MB-231 cells were seeded into a ULA microplate at a density of 4000 per well and the spheroids were formed using the same procedure as previously discussed. Cell culture medium was replaced with the medium containing free DTX, DTX-loaded crosslinked or un-crosslinked MLNPs at concentration of 7 μg mL^{-1} (of DTX) or medium in the absence of MLNPs (controls were prepared as described in the previous section) and the spheroids were incubated for 24 h at 37 °C in 5% CO_2. After the incubation, supernatants were collected and the spheroids were dissociated using TrypLE. The resultant single cell suspensions from six wells per condition were pooled together in a microcentrifuge tube and cells were centrifuged and washed with PBS 3 times. Cells were then resuspended and transferred to the flow cytometry tubes. CellEvent™ caspase-3/7 Green Detection reagent at the concentration of 500 μM was added to the tubes (1 μL) and cells were incubated for 30 minutes at 37 °C protected from light. After 25 minutes of incubation, 1 μL SYTOX™ AADvanced red at a concentration of 1 mM was added and cells were incubated for a further 5 minutes at 37 °C. Samples were then analysed without washing or fixing using a Beckman Coulter FC 500 flow cytometer and data were analysed using Kaluza 1.5 software.

4.10. Western blotting and immunodetection

Proteins separated on SDS-PAGE gels for western blotting were transferred to nitrocellulose membranes by electrophoresis in 1× transfer buffer using wet transfer apparatus (Bio-Rad). Membranes were stained in 1% Ponceau S solution and washed with sterile water to verify transfer efficiency. Nitrocellulose membranes containing immobilised proteins were incubated in blocking buffer for 1 hour at room temperature to block non-specific antibody binding sites. Membranes were then incubated with primary antibody (Anti-BCRP/ABCG2 antibody [EPR20080] – Abcam and Anti-beta Tubulin antibody (ab179513) – Abcam) at 4 °C overnight. Primary antibody was prepared in blocking buffer at dilutions 1 : 1000. The nitrocellulose membrane was washed three times (3 × 5 minutes) in 1× PBS containing 0.1% (v/v) Tween 20, prior to incubation with 1 : 3000 secondary antibody (HRP goat anti-Rabbit IgG-HRP: Catalog # 31460 – ThermoFisher Scientific) for 90 minutes at room temperature. The excess secondary antibody was removed by three more washes (3 × 5 minutes) in 1× PBS containing 0.1% Tween 20. Protein antibody complexes were detected by Enhanced chemiluminescence (ECL). The chemiluminescent signal was detected using a luminescent image analyser (Fujifilm LAS-4000).

4.11. Statistical analysis

Statistical significances were determined using *t*-test or analysis of variance (one-way and two-way ANOVA). Values of $p < 0.05$ were considered statistically significant.

Author contributions

Cíntia J. Monteiro: Data curation, formal analysis, investigation, methodology, validation, visualization, writing – orig-

inal draft, writing – review & editing. Patrícia F. Monteiro: Conceptualization, data curation, formal analysis, investigation, methodology, validation, visualization, writing – original draft, writing – review & editing. Alessandra Travanut: Investigation, methodology, validation. Muhammad Gulfam: Investigation, methodology, validation. David M. Heery: Project administration, resources, supervision, writing – review & editing. Anna Grabowska: Project administration, resources, supervision, writing – review & editing. Cameron Alexander: Conceptualization, funding acquisition, methodology, project administration, supervision, writing – review & editing.

Data availability

The data supporting this article, including microscopy images, FACS data and raw gel images for Western blots, have been included as part of the ESI† or are available from the corresponding authors Cameron Alexander and Patricia Monteiro.

Conflicts of interest

There are no conflicts of interest to declare.

Acknowledgements

We thank EPSRC for funding [Grants EP/N006615/1, EP/H005625/1, EP/N03371X/1], the Royal Society [Wolfson Research Merit Award WM150086 to CA], and CAPES (Coordenação de Aperfeiçoamento de Pessoal de Nível Superior – Brazil) for the PhD scholarships (PM and CM). We also thank the European Commission, Education, Audiovisual and Cultural Executive Agency, (EACEA) for an Erasmus Mundus grant to MG (NanoFar Joint Doctoral Program). We thank the Nottingham Breast Cancer Research Centre for invaluable support. We acknowledge Dr Rory de Brito and Dr David Onion for expert assistance in FACS data analysis. We also thank Carol Turrill for outstanding administrative support and Douglas Crackett, Esme Ireson and Paul Cooling for expert technical support. The Nanoscale & Microscale Research Centre (NMRC) is acknowledged for providing the facilities for TEM analysis and access to instrumentation. We also thank the School of Life Sciences Imaging facility (SLIM) and their staff, particularly Dr Tim Self, for use of their facilities.

References

1 G. Szakacs, J. K. Paterson, J. A. Ludwig, C. Booth-Genthe and M. M. Gottesman, *Nat. Rev. Drug Discovery*, 2006, **5**, 219–234.
2 K. O. Alfarouk, C. M. Stock, S. Taylor, M. Walsh, A. K. Muddathir, D. Verduzco, A. H. Bashir, O. Y. Mohammed, G. O. Elhassan, S. Harguindey, S. J. Reshkin, M. E. Ibrahim and C. Rauch, *Cancer Cell Int.*, 2015, **15**, 71.
3 L. Zhou, H. Wang and Y. Li, *Theranostics*, 2018, **8**, 1059–1074.
4 C. M. Perou, T. Sorlie, M. B. Eisen, M. van de Rijn, S. S. Jeffrey, C. A. Rees, J. R. Pollack, D. T. Ross, H. Johnsen, L. A. Akslen, O. Fluge, A. Pergamenschikov, C. Williams, S. X. Zhu, P. E. Lonning, A. L. Borresen-Dale, P. O. Brown and D. Botstein, *Nature*, 2000, **406**, 747–752.
5 X. Dong and R. J. Mumper, *Nanomedicine*, 2010, **5**, 597–615.
6 H. Lage, *Int. J. Antimicrob. Agents*, 2003, **22**, 188–199.
7 S. V. Ambudkar, S. Dey, C. A. Hrycyna, M. Ramachandra, I. Pastan and M. M. Gottesman, *Annu. Rev. Pharmacol. Toxicol.*, 1999, **39**, 361–398.
8 H. Yao, G. He, S. Yan, C. Chen, L. Song, T. J. Rosol and X. Deng, *Oncotarget*, 2016, **8**, 1913–1924.
9 R. D. Chacon and M. V. Costanzo, *Breast Cancer Res.*, 2010, **12**(Suppl 2), S3.
10 A. K. Pearce, A. B. Anane-Adjei, R. J. Cavanagh, P. F. Monteiro, T. M. Bennett, V. Taresco, P. A. Clarke, A. A. Ritchie, M. R. Alexander, A. M. Grabowska and C. Alexander, *Adv. Healthc. Mater.*, 2020, **9**, e2000892.
11 V. Taresco, T. F. Abelha, R. J. Cavanagh, C. E. Vasey, A. B. Anane-Adjei, A. K. Pearce, P. F. Monteiro, K. A. Spriggs, P. Clarke, A. Ritchie, S. Martin, R. Rahman, A. M. Grabowska, M. B. Ashford and C. Alexander, *Adv. Ther.*, 2021, **4**, 2000103.
12 G. Mustacchi and M. De Laurentiis, *Drug Des., Dev. Ther.*, 2015, **9**, 4303–4318.
13 C. Kim, R. Gao, E. Sei, R. Brandt, J. Hartman, T. Hatschek, N. Crosetto, T. Foukakis and N. E. Navin, *Cell*, 2018, **173**, 879–893.
14 K. Alamoudi, P. Martins, J. G. Croissant, S. Patil, H. Omar and N. M. Khashab, *Nanomedicine*, 2017, **12**, 1421–1433.
15 O. S. Muddineti, P. Kumari, E. Ray, B. Ghosh and S. Biswas, *Nanomedicine*, 2017, **12**, 1435–1453.
16 X. Jin, R. Mo, Y. Ding, W. Zheng and C. Zhang, *Mol. Pharmaceutics*, 2014, **11**, 145–157.
17 L. L. Song, Q. Jiang, J. B. Liu, N. Li, Q. Liu, L. R. Dai, Y. Gao, W. L. Liu, D. S. Liu and B. Q. Ding, *Nanoscale*, 2017, **9**, 7750–7754.
18 A. Travanut, P. F. Monteiro, S. Oelmann, S. M. Howdle, A. M. Grabowska, P. A. Clarke, A. A. Ritchie, M. A. R. Meier and C. Alexander, *Macromol. Rapid Commun.*, 2021, 2000321.
19 P. F. Monteiro, A. Travanut, C. Conte and C. Alexander, *WIREs Nanomed. Nanobiotechnol.*, 2021, **13**, e1678.
20 A. Beatty, L. S. Fink, T. Singh, A. Strigun, E. Peter, C. M. Ferrer, E. Nicolas, K. Q. Cai, T. P. Moran, M. J. Reginato, U. Rennefahrt and J. R. Peterson, *Mol. Cancer Ther.*, 2018, **17**, 264–275.
21 T. Miran, A. T. J. Vogg, N. Drude, F. M. Mottaghy and A. Morgenroth, *FASEB J.*, 2018, **32**, 2803–2813.
22 R. R. Perry, J. Mazetta, M. Levin and S. C. Barranco, *Cancer*, 1993, **72**, 783–787.
23 P. F. Monteiro, M. Gulfam, C. J. Monteiro, A. Travanut, T. F. Abelha, A. K. Pearce, C. Jerome, A. M. Grabowska, P. A. Clarke, H. M. Collins, D. M. Heery, P. Gershkovich and C. Alexander, *J. Controlled Release*, 2020, **323**, 549–564.

24 T.-M. Achilli, J. Meyer and J. R. Morgan, *Expert Opin. Biol. Ther.*, 2012, **12**, 1347–1360.
25 C. Dubois, R. Dufour, P. Daumar, C. Aubel, C. Szczepaniak, C. Blavignac, E. Mounetou, F. Penault-Llorca and M. Bamdad, *Oncotarget*, 2017, **8**, 95316–95331.
26 A. Nagelkerke, J. Bussink, F. C. G. J. Sweep and P. N. Span, *Anal. Biochem.*, 2013, **437**, 17–19.
27 J. Friedrich, C. Seidel, R. Ebner and L. A. Kunz-Schughart, *Nat. Protoc.*, 2009, **4**, 309–324.
28 A. S. Mikhail, S. Eetezadi and C. Allen, *PLoS One*, 2013, **8**, e62630.
29 S. Sant and P. A. Johnston, *Drug Discovery Today: Technol.*, 2017, **23**, 27–36.
30 J. D. Simpson, P. F. Monteiro, G. R. Ediriweera, A. R. Prior, S. E. Sonderegger, C. A. Bell, N. L. Fletcher, C. Alexander and K. J. Thurecht, *ACS Appl. Bio Mater.*, 2021, **4**, 2675–2685.
31 L. Doyle and D. D. Ross, *Oncogene*, 2003, **22**, 7340–7358.
32 A. Haimeur, G. Conseil, R. G. Deeley and S. P. Cole, *Curr. Drug Metab.*, 2004, **5**, 21–53.
33 Q. Mao and J. D. Unadkat, *AAPS J.*, 2005, **7**, E118–E133.
34 Q. Mao and J. D. Unadkat, *AAPS J.*, 2015, **17**, 65–82.
35 Y. Xie, K. Xu, D. E. Linn, X. Yang, Z. Guo, H. Shimelis, T. Nakanishi, D. D. Ross, H. Chen, L. Fazli, M. E. Gleave and Y. Qiu, *J. Biol. Chem.*, 2008, **283**, 3349–3356.
36 K. M. Sobek, J. L. Cummings, D. J. Bacich and D. S. O'Keefe, *Exp. Cell Res.*, 2017, **354**, 40–47.
37 P. Longati, X. Jia, J. Eimer, A. Wagman, M. R. Witt, S. Rehnmark, C. Verbeke, R. Toftgard, M. Lohr and R. L. Heuchel, *BMC Cancer*, 2013, **13**, 95.
38 S. Ghosh, G. C. Spagnoli, I. Martin, S. Ploegert, P. Demougin, M. Heberer and A. Reschner, *J. Cell Physiol.*, 2005, **204**, 522–531.
39 F. Perche and V. P. Torchilin, *Cancer Biol. Ther.*, 2012, **13**, 1205–1213.
40 S. Breslin and L. O'Driscoll, *Drug Discovery Today*, 2013, **18**, 240–249.
41 C. Momoli, B. Costa, L. Lenti, M. Tubertini, M. D. Parenti, E. Martella, G. Varchi and C. Ferroni, *Cancers*, 2025, **17**(4), 700.
42 M. E. Katt, A. L. Placone, A. D. Wong, Z. S. Xu and P. C. Searson, *Front. Bioeng. Biotechnol.*, 2016, **4**, 12.
43 K. Kageyama, M. Ohara, K. Saito, S. Ozaki, M. Terai, M. J. Mastrangelo, P. Fortina, A. E. Aplin and T. Sato, *J. Transl. Med.*, 2017, **15**, 145.
44 L. Austin Doyle and D. D. Ross, *Oncogene*, 2003, **22**, 7340–7358.
45 R. W. Robey, K. M. Pluchino, M. D. Hall, A. T. Fojo, S. E. Bates and M. M. Gottesman, *Nat. Rev. Cancer*, 2018, **18**, 452–464.